







Temperature-dependent study of the spin dynamics of coupled $\text{Y}_3\text{Fe}_5\text{O}_{12}/\text{Gd}_3\text{Fe}_5\text{O}_{12}/\text{Pt}$ trilayers

Felix Fuhrmann , Sven Becker , Akashdeep Akashdeep , and Gerhard Jakob 
Institute of Physics, University of Mainz, Staudingerweg 7, Mainz 55128, Germany

Qianqian Lan, Nan Wang, and Rafal E. Dunin-Borkowski
*Ernst Ruska-Centre for Microscopy and Spectroscopy with Electrons (ER-C-1),
 Forschungszentrum Jülich GmbH, 52425 Jülich, Germany*

Romain Lebrun 
Laboratoire Albert Fert, CNRS, Thales, Université Paris Saclay, F-91767 Palaiseau, France

Mathias Weiler ^{*}
*Fachbereich Physik and Landesforschungszentrum OPTIMAS,
 Rheinland-Pfälzische Technische Universität Kaiserslautern-Landau, 67663 Kaiserslautern, Germany*

Mathias Kläui [†]
*Institute of Physics, University of Mainz, Staudingerweg 7, Mainz 55128, Germany;
 Graduate School of Excellence "Materials Science in Mainz" (MAINZ), Staudingerweg 9, Mainz 55128, Germany;
 and Center for Quantum Spintronics, Department of Physics, Norwegian University of Science and Technology, Trondheim 7491, Norway*



(Received 30 January 2025; revised 2 July 2025; accepted 9 July 2025; published 22 August 2025)

We combine ferromagnetic resonance absorption measurements (FMR) with spin pumping measurements to ascertain the full magnetization dynamics of $\text{Y}_3\text{Fe}_5\text{O}_{12}$ (YIG)/ $\text{Gd}_3\text{Fe}_5\text{O}_{12}$ (GdIG)/Pt heterostructures. This trilayer system offers the unique possibility to individually investigate the spin dynamics of the ferrimagnetic GdIG close to its compensation temperature. We show that this trilayer acts as a highly tunable spin current source and our experimental results are corroborated by micromagnetic simulations. The detected spin current in the top Pt layer is governed by spin dynamics in the GdIG layer, while the broadband FMR absorption spectrum of the full heterostructure comprises contributions from spin dynamics in both layers. Thus, combining the measurements of FMR absorption and spin current generation from the spin pumping and spin Seebeck effect allows us to understand the spin dynamics contributions of both constituents.

DOI: [10.1103/7d4q-j8cl](https://doi.org/10.1103/7d4q-j8cl)

I. INTRODUCTION

In recent years, the field of magnonics has been rapidly developing. Encoding information by spin angular momentum instead of moving charge carriers can potentially decrease energy consumption [1,2]. This fuels interest in developing magnonic devices, which can be used for magnon logic operations and offer potentially increased speed and lower power consumption [1,3]. Rare-earth garnets such as $\text{Y}_3\text{Fe}_5\text{O}_{12}$ (YIG) offer a unique platform with long-distance magnon propagation, enabled by its low Gilbert damping constant of down to $\alpha \approx 10^{-5}$ [4–7]. $\text{Gd}_3\text{Fe}_5\text{O}_{12}$ (GdIG) is a compensated ferrimagnetic rare-earth garnet with a temperature-dependent net magnetization that vanishes at the magnetic moment compensation temperature in the bulk of $T_{\text{Comp}} \approx 295$ K [8]. Heterostructures of these materials provide an interesting static magnetic system and allow one to study the spin dynamics of the coupled heterostructure [9–11]. Currently, the

study of antiferromagnets and, in general, antiferromagnetically coupled systems is an active research area, as it promises materials with resilience against external magnetic fields perturbations, long-distance spin transport, and naturally high resonance frequencies [12,13]. Antiferromagnet-ferromagnet heterostructures [14] and ferrimagnetic systems, especially close to their compensation temperature, provide an exciting platform to study antiferromagnetic (and antiferromagnetically coupled) spin dynamics with accessible magnetic properties for each of the individual constituents [15–18]. Until now, the investigation of the dynamics of ferrimagnets close to their compensation temperature has been challenging [19,20]. However, the coupling to a second layer can potentially be used to facilitate such studies.

In this study, we experimentally investigate a YIG/GdIG/Pt thin-film heterostructure, as schematically depicted in Fig. 1(a). We observe a strong impact of the magnetic configuration of the individual layers of our heterostructure on the spin dynamics, spin pumping, and spin Seebeck effect signals. We show that the generated spin current originates from the GdIG layer, which provides a unique opportunity to investigate the GdIG spin dynamics

^{*}Contact author: weiler@physik.uni-kl.de

[†]Contact author: klaui@uni-mainz.de

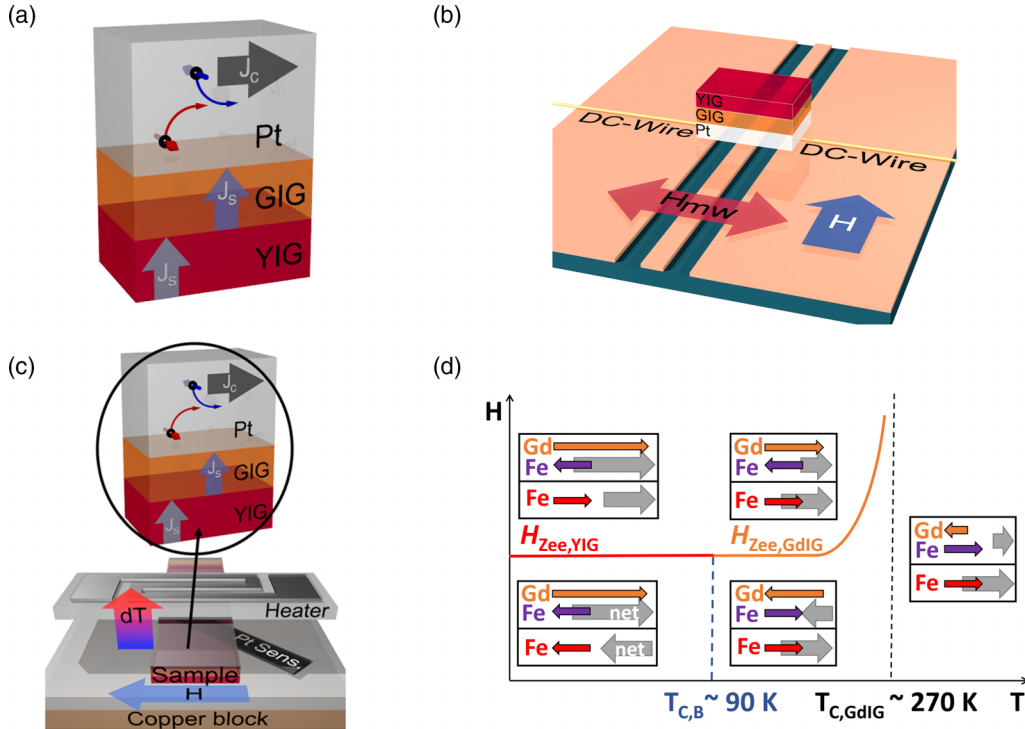


FIG. 1. (a) Illustration of the YIG/GdIG/Pt trilayer (the GGG substrate is not shown). The spin current J_S , which is potentially generated by both the YIG and GdIG layers, is converted into a charge current J_C in the Pt layer via the iSHE. (b) Illustration of the sample positioning on a CPW. The sample is connected with two thin wires, on the left and right side. The voltage V_{iSHE} , generated in the Pt layer of the sample, is measured by a lock-in technique. (c) Illustration of the SSE sample stack with a constant temperature gradient. The temperature gradient is established between the Pt heater on top of the sample and the copper piece (in contact with the VTI of the cryostat). The gradient is estimated by comparing the resistance of the Pt heater and Pt sensor below the sample. The zoomed-in section illustrates the iSHE in the Pt after a spin current is channeled into the Pt top layer. (d) Illustration of the YIG/GdIG/Pt trilayer alignment and switching field as a function of temperature with the information from Ref. [9]. Orange arrows depict the Gd sublattice, and the red (purple) arrows illustrate the direction of the combined Fe sublattices of YIG (GdIG). The H_{Zee} line indicates the approximate temperature dependence of the magnetic field necessary to switch the respective layer.

individually, aided by the coupling to the YIG layer, close to the compensation temperature. This temperature range is usually difficult to study because of the diverging linewidth of single GdIG layers at T_{Comp} [19]. Furthermore, we study the spin current generation in our system, which is tunable by temperature, external field, and relative layer thickness [9]. We drive the ferromagnetic resonance (FMR) modes of our heterostructure and measure the spin current which is pumped across the GdIG/Pt interface when a resonance condition is satisfied [21,22]. This spin current, resulting from the spin pumping (SP), is detected by means of the inverse spin Hall effect (iSHE) in the Pt top layer [23] in the experimental configuration sketched in Fig. 1(b). We obtain unique information about the switching behavior of our GdIG layer by observing the spin Seebeck effect (SSE) [24]. The SSE measurements are performed by applying an out-of-plane thermal gradient, as depicted in Fig. 1(c) [25]. We compare these results with SSE measurements, in which the gradient is generated by microwave heating during the SP measurements [26]. The microwave-induced SSE is a key tool as a measure to determine the switching of the top GdIG layer during the SP measurement itself, and is less susceptible to temperature mismatch compared to remounting the sample in another setup.

II. SAMPLE CHARACTERISTICS

The investigated sample is a trilayer of YIG, GdIG, and Pt, grown on a $\text{Gd}_3\text{Ga}_5\text{O}_{12}$ (GGG) (001) substrate. The thicknesses of the YIG and GdIG layers are chosen to be 36 nm and 30 nm, respectively. The coupling between YIG and GdIG moments was previously studied in Ref. [9]. The YIG and GdIG films are grown in a pulsed laser deposition chamber. The substrates are (001)-oriented GGG. The chamber operates at an ultrahigh vacuum with a base pressure of 2×10^{-8} mbar. Laser pulses with an energy of 130 mJ per pulse and a wavelength of 248 nm are used at a repetition rate of 10 Hz. During growth, the chamber conditions are a substrate temperature of 475 °C and an O_2 pressure of 0.026 mbar. The thickness is determined by the number of laser pulses used for the deposition. These films show high crystallinity and sharp interfaces, which can be resolved in high-angle annular dark-field (HAADF) scanning transmission electron microscopy (STEM). The high-resolution image at the YIG/GdIG interface is provided in Fig. 2 of the Supplemental Material (SM) [27]. The STEM images and film quality are discussed in more detail in the SM [27].

The relative alignment of the YIG and GdIG layer magnetizations is investigated by superconducting quantum

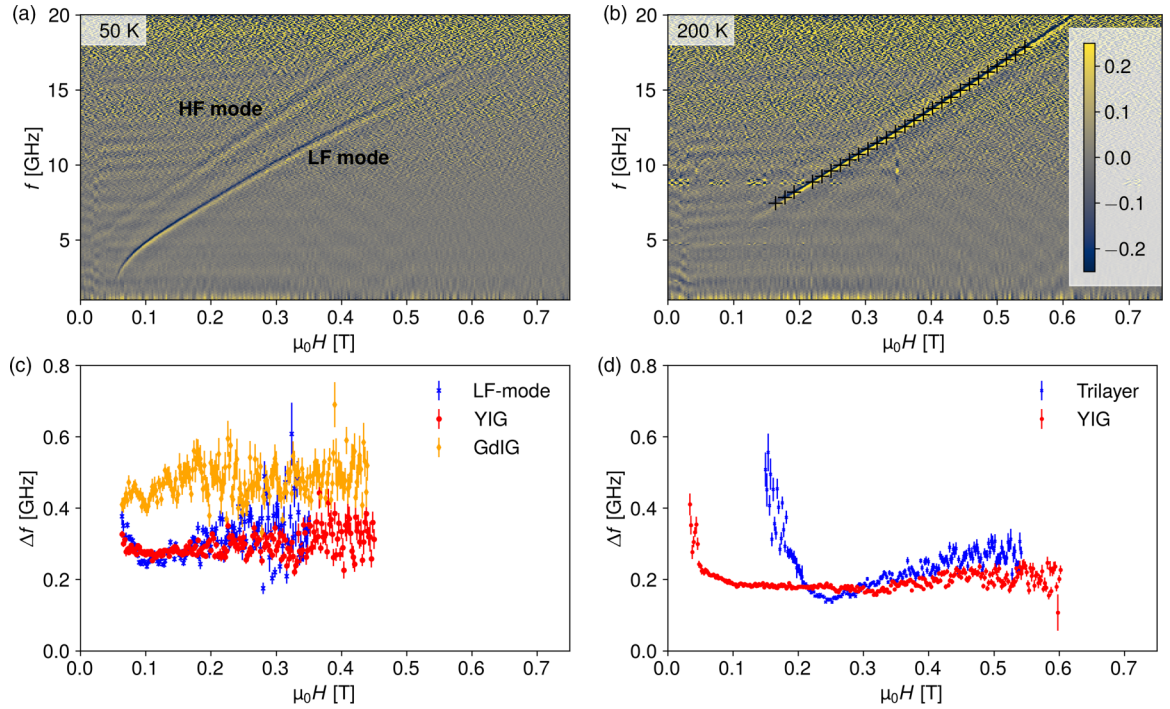


FIG. 2. (a) Broadband VNA-FMR measurement of the YIG 36 nm/GdIG 30 nm/Pt 4 nm trilayer at 50 K. The raw data are processed by derivative divide and an fast Fourier transform (FFT) filter. The resonance linewidth is extracted by fitting to the derivative of the susceptibility for N resonances [28]. (b) Broadband VNA-FMR spectrum measurement at 200 K. The raw data are processed by derivative divide and an FFT filter, which filters signals by frequency apart from an allowed window. The resonance linewidth is extracted by fitting to the derivative of susceptibility for N resonances [14,28]. (c) The linewidth at 50 K from the YIG 36 nm/Pt 4 nm and GdIG 30 nm samples (red and orange, respectively) and the trilayer LF mode (blue) in comparison. We provide the color map of the GdIG thin film in Fig. 1 of the SM [27]. (d) Extracted linewidth at 200 K from the trilayer and a pure YIG sample in comparison.

interference device (SQUID) magnetometry and spin Hall magnetoresistance [9,10]. With this information and the (microwave-induced) SSE measurements, we can determine the relative alignment of the layer magnetizations in our sample. Figure 1(d) shows an illustration of the switching field (and thus relative alignment) as a function of temperature for the YIG 36 nm/GdIG 30 nm/Pt 4 nm sample. For temperatures below the bilayer compensation temperature $T_{C,B}$, the net moment of the GdIG layer, $M_{\text{net,GdIG}}$, is larger than the one of the YIG layer, $M_{\text{net,YIG}}$. At $T_{C,B}$, the two layers have the same net moment, which are antiferromagnetically coupled via the Fe-Fe sublattices [9,10] and thus fully compensate each other. For temperatures above $T_{C,B}$ and below $T_{C,\text{GdIG}}$ (the compensation temperature of single-layer GdIG), the net moment of the YIG layer, $M_{\text{net,YIG}}$, is larger than that of the GdIG layer, $M_{\text{net,GdIG}}$. Under small external applied in-plane magnetic fields, the net magnetization of both layers is parallel to the applied field, while the individual layer magnetizations are antiparallel. For larger external magnetic fields, the Zeeman energy exceeds the exchange coupling between the layers, and the layer with the smaller net moment also switches so that both magnetizations are parallel with the external magnetic field. While the net moments $M_{\text{net,GdIG}}$ and $M_{\text{net,YIG}}$ are antiferromagnetically aligned below $T_{C,\text{GdIG}}$, the two-layer magnetizations $M_{\text{net,GdIG}}$ and $M_{\text{net,YIG}}$ are always parallel above $T_{C,\text{GdIG}}$. The results of this trilayer structure are compared to the FMR data of a single GdIG layer of

a comparable thickness of 30 nm and a YIG 36 nm/Pt 4 nm bilayer film. Having thus established the static magnetization configurations of the multilayer heterostructure, we next study the dynamics.

III. RESULTS AND DISCUSSION

A. Ferromagnetic resonance absorption

The ferromagnetic resonance measurements are key to understanding the dynamic behavior of our system. With the FMR measurements, we can identify features originating from each layer, but also understand the underlying coupling of the heterostructure. To obtain FMR color maps, as shown in Figs. 2(a) and 2(b), we use a vector network analyzer (VNA) to measure the microwave absorption of the sample. In this case, the frequency is swept by the VNA for each external magnetic field step $\mu_0\mathbf{H}$, resulting in a broadband FMR measurement (bbFMR) [29]. The obtained raw data are then processed by the derivative Divide (dD) algorithm following the work of Maier-Flaig *et al.* [30],

$$d_D S_{21} = \frac{S_{21}(\omega, H_0 + \Delta H_{\pm}) - S_{21}(\omega, H_0 - \Delta H_{\pm})}{S_{21}(\omega, H_0) \Delta H_{\pm}} \quad (1)$$

$$\approx -i\omega A' \frac{d\chi}{d\omega}. \quad (2)$$

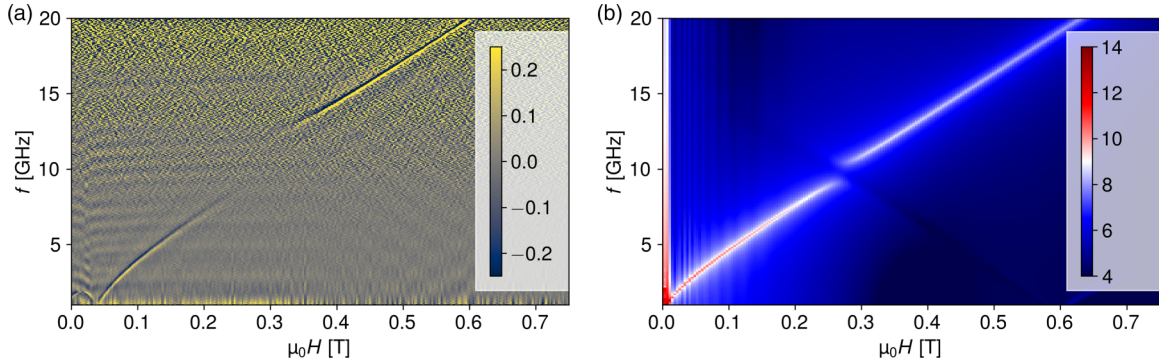


FIG. 3. (a) Broadband VNA-FMR measurement of the YIG 36 nm/GdIG 30 nm/Pt 4 nm trilayer at 250 K. The raw data are processed by derivative divide and an FFT filter. The resonance linewidth is extracted by fitting it to the derivative of the susceptibility for N resonances [28]. (b) FMR spectrum of the micromagnetic simulation. The magnetization is estimated from the literature to match a temperature of 265 K to compare to the thin film at 250 K as the bulk compensation temperature is shifted compared to the value for our thin films.

Here, $d_{\text{D}}S_{21}$ is thus effectively the normalized derivative of the S_{21} parameter (transmission parameter) with respect to the magnetic field [30]. Equation (2) contains the magnetic susceptibility $\chi(\omega, H_0)$ and the signal amplitude A' ,

$$\chi(\omega, H_0) = \frac{\omega_M(\gamma\mu_0 H_0 - i\Delta\omega)}{[\omega_{\text{res}}(H_0)]^2 - \omega^2 - i\omega\Delta\omega}, \quad (3)$$

with $\omega_M = \gamma\mu_0|M|$, the resonance angular frequency ω_{res} , and the gyromagnetic ratio γ [30].

In our FMR measurements, we compare VNA-FMR color maps recorded at different temperatures. We measured our single-layer YIG and GdIG films first to compare them later to the features of our heterostructure [Figs. 2(c) and 2(d)].

For the heterostructure, the signal differs strongly in its shape and temperature dependence from those of the single layers. For a temperature of $50 \text{ K} < T_{\text{C,B}}$ [see Fig. 1(d)], we observe two distinct modes, one at lower and one at higher frequencies [Fig. 2(a)]. Both modes do not behave as one would expect from the Kittel equation for in-plane applied external magnetic fields for single layers, which we attribute to their coupling. However, the linewidth and signal strength of the mode at lower frequencies (LF mode) are closer to that obtained for the YIG single layer [Fig. 2(c)]. The increase of the slope of the mode towards lower temperatures was also previously observed for GdIG [31]. The higher-frequency mode (HF mode) resembles the behavior of the single GdIG layer. However, for temperatures in which the two modes are close to each other [see Figs. 2(b) and 3(a)], it becomes clear that the behavior is increasingly complex, making it more challenging to disentangle the modes for the bilayer system. At $200 \text{ K} > T_{\text{C,GdIG}}$, we observe a merged resonance line [Fig. 2(b)], which we attribute to the detection of the YIG FMR as corroborated by the resonance field and linewidth [Fig. 2(d)]. The pronounced change of the linewidth during the field sweep for the trilayer system can be explained by the coupled dynamics between the YIG and GdIG layers. To identify the features and investigate their origin in more detail, we next complement the FMR absorption data with micromagnetic simulations, and SP and SSE measurement results.

B. Micromagnetic simulation

The data from our experiments at an increased temperature of 250 K are next compared to micromagnetic simulations [Figs. 3(a) and 3(b)] to understand the observed features of the measurements of the spin dynamics. The simulations were conducted using MUMAX³ [32] via the UBERMAG metapackage [33] written for PYTHON with small modifications. Our micromagnetic approach can be compared to a macrospin model (see Fig. 4 of the SM [27]; see, also, Ref. [34] in the SM [27]). From this comparison, we find that the micromagnetic simulation captures the experimental features in more detail and provides more information about the static magnetic states, especially during the switching process. The initial parameters for the simulation are set by the literature values [15,35–37]. We assume the damping parameter α_{YIG} to be 3×10^{-3} , which we extracted from single-layer YIG measurements (see the SM [27] and Fig. 3 of the SM [27]; see, also, Ref. [38] in the SM [27]), and compatible with that expected for pulsed laser deposition (PLD)-grown YIG samples [39]. The GdIG damping is estimated to be 5×10^{-2} from Ref. [19]. The magnetization of each layer is estimated from the literature values for a set temperature [40]. An interfacial coupling between YIG and GdIG is expected and estimated from the exchange constant, determined in Ref. [9]. The result of such a simulation is shown in Fig. 3(b). The overall signal shape reproduces our FMR spectrum well [see Figs. 3(a) and 3(b) for measurements at 250 K]. The exchange-driven mode [41,42] with negative frequency to field dispersion appears to be only a weak signal, in simulation and experiment. However, the effect of its anticrossing with the main mode is very conspicuously captured by the measurements (see Fig. 3, and Fig. 5 of the SM [27]). As the static magnetic state of the system is crucial to the dynamics, we compare the SSE measurements and magnetization curve extracted from the simulation in Fig. 6 of the SM [27]. The micromagnetic simulations also suggest a helical spin structure in the GdIG layer during and after the switching (see Fig. 7 of the SM [27]), which supports the previous conclusion by Ref. [10] of a spiral magnetization state.

To explain the switching behavior and the dynamic response of the heterostructure, we next use the SSE as a tool to

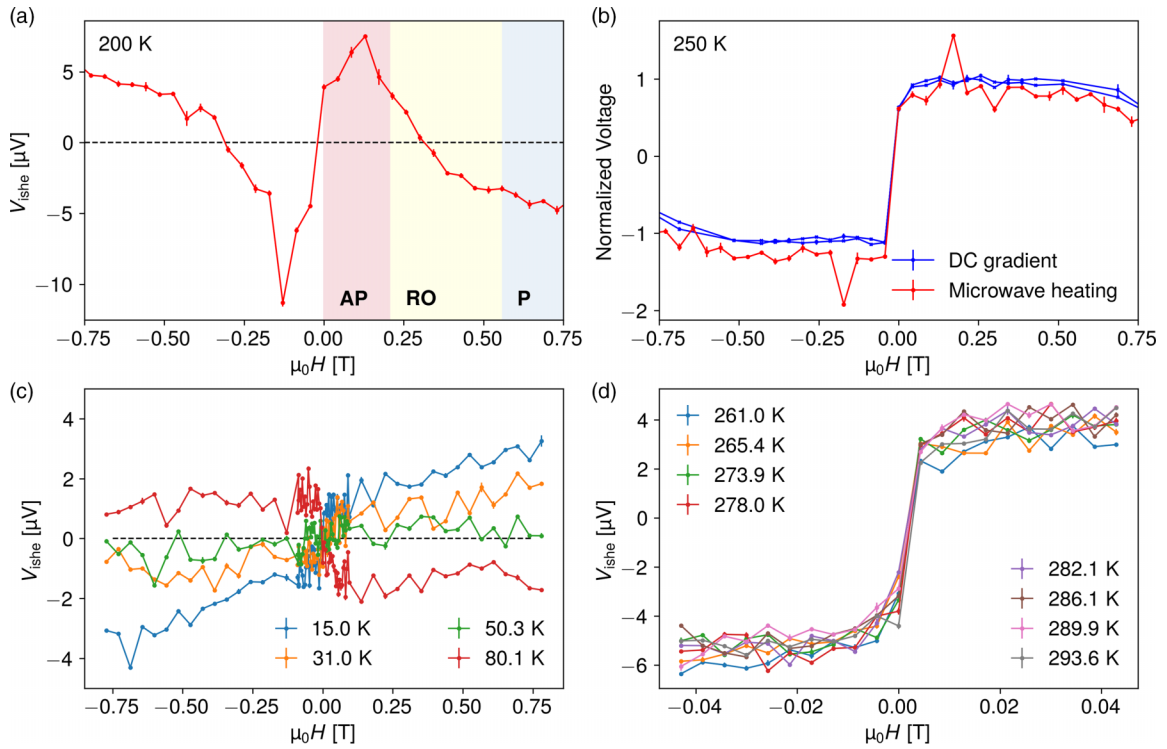


FIG. 4. (a) The SSE measurement by microwave heating at 200 K of the trilayer. A constant offset is subtracted. The dashed line helps as a guide to the eye to clarify the switching behavior. The error bars show the standard error of the average over 15 data points per field step. The background colors of the plot (red, yellow, and blue, respectively) refer to the ranges in which the GdIG layer is antiparallel (AP), reorienting (RO), and parallel (P) to the magnetic field. (b) Spin Seebeck effect measurements by microwave heating and DC heating with a resistive heater attached to the sample at 250 K, where both indicate the start of the reorientation of the top GdIG layer above 0.5 T. The reorientation continues to higher fields > 2 T. (c) V_{SHE} of the SSE by microwave heating for low temperatures, with the DC voltage offset subtracted [24,43,44]. (d) The low-field step of V_{SHE} has its origin in the spin Seebeck effect. The observed SSE signal shows no sign change, in contrast to the SP signal over the same temperature range as in (a).

probe the relative alignment of the YIG and GdIG layers. The SSE also provides a complementary approach to spin current generation in the sample via a temperature gradient.

C. Spin Seebeck effect measurement

The SSE measurements performed in the course of this study give important insight into the static magnetic state of the system for the respective applied external magnetic field [43]. The YIG contribution to the SSE signal is heavily attenuated, thus providing us with just the information about the GdIG top layer [9].

We compare the SSE signal caused by microwave heating with the SSE signal from a simple continuous temperature gradient to verify the field dependence of the SSE signal, which is measured during the application of the FMR [Fig. 4(b)]. For the latter, the sample is clamped in between a cold sink, on which a Pt stripe is attached, and a resistive Pt heater, as implemented in Ref. [43] [Fig. 1(c)]. When applying a current to the top Pt heater, a temperature gradient is established perpendicular to the sample plane. The voltage, which builds up on the sample, is measured with an HP 34420A nanovoltmeter. For the SSE signal during the microwave application, we measure the V_{SHE} during the field sweep. By applying a sufficiently strong microwave power, we coincidentally heat the film, additionally inducing the spin

Seebeck effect [45,46]. This background signal is dependent on the magnetization direction of the GdIG layer, which provides us with a direct comparison between the switching state of the top layer and the FMR signal. This signal includes the distinct peak attributed to spin pumping (SP) at resonance (at $\mu_0 H \approx 0.15$ T); see Figs. 4(a) and 4(b). When we compare it to the DC-SSE, we can see a good agreement in the field dependence (apart from the aforementioned SP-signal peak at FMR).

As observed in Ref. [9], the SSE signal is dominated by the GdIG top layer. The SSE signal probes thermally excited magnons of all wavelengths, while FMR leads to wave-vector $\mathbf{k} = 0$ magnon excitations. This means that for the appropriate temperature range, we can detect the reorientation process during the field sweep of the GdIG layer. We do not observe a clear contribution of the YIG bottom layer, even if a superposition of spin currents could appear in our SSE measurements [3,47]. Our results indicate that the spin current generated in the YIG layer cannot penetrate across the GdIG layer due to its larger damping and the interface between YIG and GdIG.

After comparison with the microwave-generated SSE, we confirm good agreement with the DC-SSE signal. For further investigations, we would mainly use the microwave-generated SSE. This enables a more direct comparison to the SP and FMR signal, as no remounting of the sample is needed.

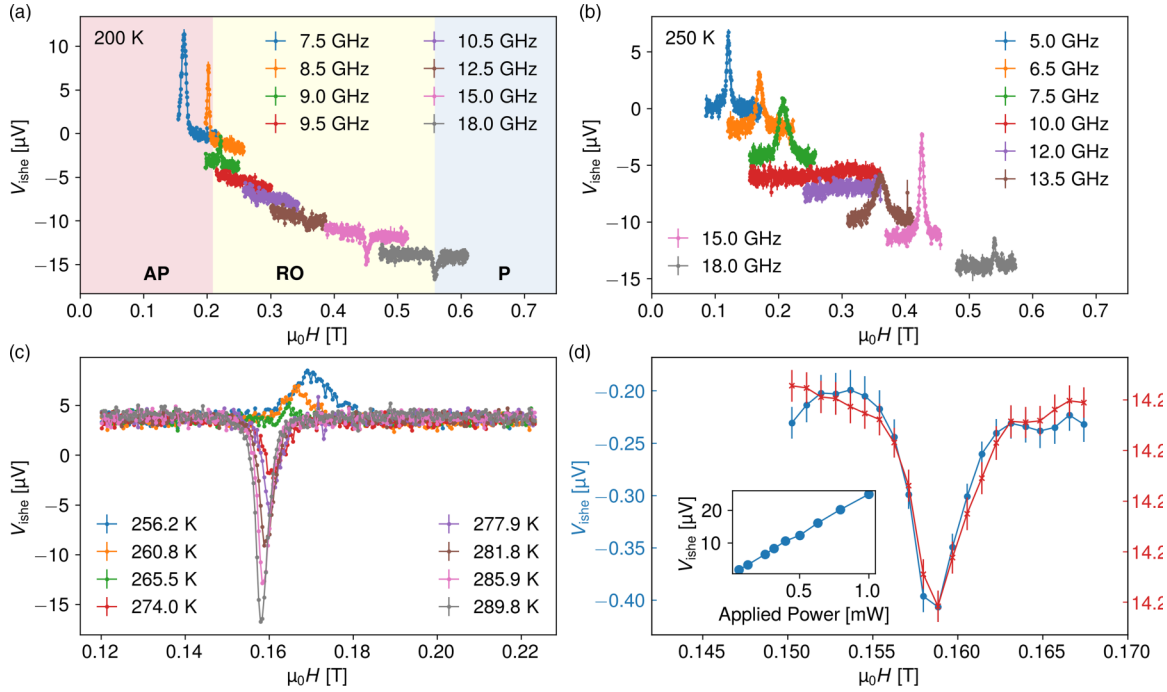


FIG. 5. (a) Measurement of V_{ISHE} from SP at resonance with different excitation frequency at 200 K. A constant offset of 2 μV is artificially added to visibly separate the signal at different frequencies. The background colors of the plot (red, yellow, and blue, respectively) refer to the ranges in which the GdIG layer is antiparallel (AP), reorienting (RO), and parallel (P) to the magnetic field. (b) Measurement of V_{ISHE} from SP at resonance with different excitation frequencies at 250 K. A constant offset of 2 μV is artificially added to separate the signal at different frequencies visibly in the plot. (c) V_{ISHE} at fixed resonance frequency of 6.5 GHz for different temperatures. The temperature range reaches across the GdIG compensation temperature. The sign of V_{ISHE} switches at $T \approx 270$ K. (d) Microwave absorption (red curve) and V_{ISHE} (blue curve) in comparison at 295 K and at 6.5 GHz. Inset: A linear power dependence of the measured V_{ISHE} with respect to the power set at the RF source.

A good indication, that the observed background signal during the microwave application indeed stems from the SSE originating from the GdIG is the sign change at low temperatures. The signal vanishes at low temperature, which agrees with the sign change of the SSE in GdIG due to a change of occupied magnon modes [Fig. 4(c)] [24]. As the microwave heating power is dependent on the microwave frequency, for the applied constant microwave power, the frequency is kept constant at $f \approx 6.5$ GHz while sweeping the magnetic field. The SSE measurements are essential to interpret the spin pumping (SP) measurements in detail by revealing the relative alignment state of the two ferrimagnetic layers in the same setup. We use this information about the static magnetization configuration that we extract from the SSE [Figs. 4(a) and 4(b)] for the interpretation of the SP signals. To this end, we include the relative orientation of GdIG and YIG net magnetizations in Fig. 5(a) encoded in the background color [red = antiparallel (AP), yellow = reorientation (RO), blue = parallel (P)].

D. Spin pumping at ferromagnetic resonance

To understand the contributions of the individual layers to the magnetization dynamics, we not only study the FMR absorption spectrum that comprises contributions from both layers, but also carry out spin pumping experiments. We detect the signal of the inverse spin Hall effect (iSHE) in the Pt top layer [22,23]. At the resonance condition, a spin current is pumped from the YIG/GdIG bilayer into the adjacent Pt layer.

This generated spin current is dominated by the spin dynamics in the GdIG layer, which offers a chance to separately investigate the GdIG layer spin dynamics. While the FMR measurements are sensitive to both the GdIG and YIG spin dynamics, the SP and SSE measurements are complementary to the FMR measurements, as they only reflect the GdIG spin dynamics. The investigation of magnetic field sweeps, especially at the switching fields of the respective layers, offers the opportunity to study the spin current origin. The sample is placed on top of the coplanar waveguide (CPW) with a thin insulating tape, so that there is no electrical contact from the CPW to the Pt film. The contacts are made by a thin copper wire and silver paste to fix the wire on the Pt layer.

The alternating current is generated by a microwave generator, which is amplified and fed into the CPW, generating an alternating magnetic field at the sample. The alternating magnetic field is modulated in its amplitude by a frequency of 30 Hz. The resulting voltage V_{ISHE} is measured in the Pt layer by a lock-in technique with a Stanford Research Systems (SR) 830 lock-in amplifier with a SR-530 pre-amplifier, improving the signal-to-noise ratio and removing artifacts in the signal due to small temperature fluctuations inside the cryostat. The measurements are performed as field sweeps with a constant frequency of the alternating field, at different temperatures. At a temperature of 200 K, we can observe a sign change of the generated signal for a sweep from low to high magnetic fields (lower and higher resonance frequencies) [see Fig. 5(a)]. In this temperature range ($T_{C,B} < T < T_{C,GdIG}$), the net

moment of the YIG layer is larger than the GdIG net magnetic moment [see Fig. 1(d)]. Thus, at low fields, the YIG layer magnetization is parallel to the magnetic field, while the GdIG magnetization is oriented antiparallel. By comparing the sign change to the indicated ranges in Fig. 5(a), one can observe the voltage sign at resonance following the GdIG orientation. It is worth noting that the FMR spectrum shows a clear resonance line during the GdIG switching [compare Fig. 2(b)]. This suggests that the YIG can still be excited during the GdIG switching, and the FMR spectrum is dominated by the YIG layer in this field range. This is supported by the narrowing of the linewidth during the GdIG switching (≈ 0.2 T to 0.5 T) [see Fig. 2(c)]. From the SSE measurements [Fig. 2(b)], it is clear that the switching is not abrupt, but occurs as a reorientation over an extended field range. In this range, the linewidth is compatible with the linewidth measured in the single YIG layer. From this, we can conclude that our measurements are not sensitive to a spin current originating from YIG in this range, as there is no signal with the expected linewidth and sign observed in the V_{ISHE} signal. From SSE measurements, we can estimate the 50% switching field value. For GdIG switched 50% (at ≈ 0.3 T), we do not see any distinct peak, supporting the assumption that there is no significant transmitted spin current from the YIG across the GdIG into the Pt. The sign change of the voltage signal can be easily explained by a reorientation of the GdIG layer magnetization. As the magnetization direction of the spin current source (the GdIG layer) inverts, the spin current polarization changes, leading to an inverted voltage V_{ISHE} [Fig. 5(a)]. For higher temperatures, there is no complete switching in our measurement window from 0 T to 0.7 T [Fig. 4(b)]. Thus, the signal sign does not invert in this field range [Fig. 5(b)].

When sweeping the temperature across $T_{C,\text{GdIG}}$, one can also expect a sign change. The GdIG net moment is inverted across the compensation temperature, as the combined moment of the Fe sublattices exceeds the Gd sublattice moment. Thus, the net magnetization direction of GdIG is inverted, leading to an inversion of the $i\text{SHE}$ voltage [see Fig. 5(c)]. This again indicates that the spin current is generated in the GdIG layer, as there is no sign change of a possible YIG-spin current expected.

This sign change from the SP-generated spin current is compatible with the net magnetization orientation of the GdIG layer, which is inverted at the compensation temperature. In contrast, the spin current generated from the SSE depends on the orientation of the Fe sublattices [24,43,44]. The orientation of the sublattices does not change across the compensation temperature due to the coupling to the YIG layer [see Fig. 1(d)], which explains the absence of this sign change in the SSE measurement of the bilayer [Fig. 4(d)] compared to previous studies [24,43].

For single GdIG layers, at $T_{C,\text{GdIG}}$ one can observe a divergence of the linewidth of the FMR signal, which makes it hard to study the dynamics of the layer close to the compensation temperature. We can extract a linewidth from Fig. 5(c), which clearly shows no such divergence of the linewidth in our case. This divergence was previously studied and linked to the relation between net angular momentum and total angular moment of the material [19,48]. However, the experimental investigation is difficult due to the decrease in signal

intensity and increasing linewidth. In our system, however, the relation between the net angular momentum and total angular momentum is shifted by the coupling to the YIG layer. Thus, close to the compensation temperature, we still observe a signal originating from the GdIG layer [Fig. 5(c)]. While the linewidth does slightly change across $T_{C,\text{GdIG}}$, it is compatible with the damping estimated in Ref. [19], supporting the approach of extracting the damping for ferrimagnetic materials close to their compensation temperature with different methods than the standard ones used for ferromagnets.

IV. CONCLUSION

In this study, we investigated the spin dynamics and spin currents in a trilayer of YIG/GdIG/Pt. With complementary measurements of the spin current from the spin Seebeck effect and spin pumping measurements at FMR, and comparison to our micromagnetic simulations, we can explain the features seen in the FMR spectrum.

Our ferrimagnets exhibit a strong coupling, which is reflected in the observed static magnetic state. We find the coupling between YIG and GdIG to be strong enough to not only facilitate the different observed antiparallel and parallel alignment states of the net magnetic moments, but also key to understanding the dynamics of the heterostructure. The spin current, pumped at the ferromagnetic resonance condition, indicates that the GdIG is the origin of the spin current, which provides the opportunity to study the GdIG layer resonance close to its compensation temperature. The coupling to the YIG layer is found to prevent the resonance linewidth of the GdIG from diverging at $T_{C,\text{GdIG}}$, in contrast to measurements of single-layer GdIG. The ferromagnetic resonance measurements at 250 K show an avoided crossing, an additional indication for the coupled dynamics of the two ferrimagnetic layers. The coupled dynamics of the system are especially of interest for further studies and applications exploiting coherent spin transport.

We show that our system can be used as a highly tunable spin current source over a large temperature and external magnetic field range. This provides a platform for more complex systems such as magnon spin valves in a fully insulating system. We envision the system to facilitate further studies of coherent spin dynamics.

ACKNOWLEDGMENTS

We thank Thomas Winkler for his technical support to perform the micromagnetic simulations. We thank Zengyao Ren for his expertise during the sample growth optimization. The work is funded by the Deutsche Forschungsgemeinschaft (DFG, German Research Foundation), Grant No. TRR 173/3 - 268565370 Spin+X (Projects No. B02, No. B13, and No. A01) and the European Union through the Horizon 2020 and Horizon Europe projects under Grant Agreement No. 101070290 (NIMFEIA), EIC Pathfinder OPEN Grant No. 101129641 (OBELIX) and ANR project ICARUS (ANR-22-CE24-0008).

DATA AVAILABILITY

The data that support the findings of this article are openly available [49].

- [1] A. Brataas, B. van Wees, O. Klein, G. de Loubens, and M. Viret, Spin insulatronics, *Phys. Rep.* **885**, 1 (2020).
- [2] A. V. Chumak, V. I. Vasyuchka, A. A. Serga, and B. Hillebrands, Magnon spintronics, *Nat. Phys.* **11**, 453 (2015).
- [3] J. Cramer, F. Fuhrmann, U. Ritzmann, V. Gall, T. Niizeki, R. Ramos, Z. Qiu, D. Hou, T. Kikkawa, J. Sinova, U. Nowak, E. Saitoh, and M. Kläui, Magnon detection using a ferromagnetic collinear multilayer spin valve, *Nat. Commun.* **9**, 1089 (2018).
- [4] X.-Y. Wei, O. A. Santos, C. H. S. Lusero, G. E. W. Bauer, J. Ben Youssef, and B. J. van Wees, Giant magnon spin conductivity in ultrathin yttrium iron garnet films, *Nat. Mater.* **21**, 1352 (2022).
- [5] A. A. Serga, A. V. Chumak, and B. Hillebrands, YIG magnonics, *J. Phys. D: Appl. Phys.* **43**, 264002 (2010).
- [6] G. Schmidt, C. Hauser, P. Trempler, M. Paleschke, and E. T. Papaioannou, Ultra thin films of yttrium iron garnet with very low damping: A review, *Phys. Stat. Sol. (b)* **257**, 1900644 (2020).
- [7] L. J. Cornelissen, J. Liu, R. A. Duine, J. B. Youssef, and B. J. van Wees, Long-distance transport of magnon spin information in a magnetic insulator at room temperature, *Nat. Phys.* **11**, 1022 (2015).
- [8] R. Pauthenet, Spontaneous magnetization of some garnet ferrites and the aluminum substituted garnet ferrites, *J. Appl. Phys.* **29**, 253 (1958).
- [9] S. Becker, Z. Ren, F. Fuhrmann, A. Ross, S. Lord, S. Ding, R. Wu, J. Yang, J. Miao, M. Kläui, and G. Jakob, Magnetic coupling in $\text{Y}_3\text{Fe}_5\text{O}_{12}/\text{Gd}_3\text{Fe}_5\text{O}_{12}$ heterostructures, *Phys. Rev. Appl.* **16**, 014047 (2021).
- [10] J. M. Gomez-Perez, S. Vélez, L. McKenzie-Sell, M. Amado, J. Herrero-Martín, J. López-López, S. Blanco-Canosa, L. E. Hueso, A. Chuvilin, J. W. A. Robinson, and F. Casanova, Synthetic antiferromagnetic coupling between ultrathin insulating garnets, *Phys. Rev. Appl.* **10**, 044046 (2018).
- [11] M. J. Roos, P. Quarterman, J. Ding, M. Wu, B. J. Kirby, and B. L. Zink, Magnetization and antiferromagnetic coupling of the interface between a 20 nm $\text{Y}_3\text{Fe}_5\text{O}_{12}$ film and $\text{Gd}_3\text{Ga}_5\text{O}_{12}$ substrate, *Phys. Rev. Mater.* **6**, 034401 (2022).
- [12] R. Lebrun, A. Ross, S. A. Bender, A. Qaiumzadeh, L. Baldrati, J. Cramer, A. Brataas, R. A. Duine, and M. Kläui, Tunable long-distance spin transport in a crystalline antiferromagnetic iron oxide, *Nature (London)* **561**, 222 (2018).
- [13] S. Baierl, J. H. Mentink, M. Hohenleutner, L. Braun, T.-M. Do, C. Lange, A. Sell, M. Fiebig, G. Woltersdorf, T. Kampfrath, and R. Huber, Terahertz-driven nonlinear spin response of antiferromagnetic nickel oxide, *Phys. Rev. Lett.* **117**, 197201 (2016).
- [14] H. Al-Hamdo, T. Wagner, Y. Lytvynenko, G. Kendzo, S. Reimers, M. Ruhwedel, M. Yaqoob, V. I. Vasyuchka, P. Pirro, J. Sinova, M. Kläui, M. Jourdan, O. Gomonay, and M. Weiler, Coupling of ferromagnetic and antiferromagnetic spin dynamics in $\text{Mn}_2\text{Au}/\text{NiFe}$ thin film bilayers, *Phys. Rev. Lett.* **131**, 046701 (2023).
- [15] L. Liensberger, A. Kamra, H. Maier-Flaig, S. Geprägs, A. Erb, S. T. B. Goennenwein, R. Gross, W. Belzig, H. Huebl, and M. Weiler, Exchange-enhanced ultrastrong magnon-magnon coupling in a compensated ferrimagnet, *Phys. Rev. Lett.* **123**, 117204 (2019).
- [16] S. Klingler, V. Amin, S. Geprägs, K. Ganzhorn, H. Maier-Flaig, M. Althammer, H. Huebl, R. Gross, R. D. McMichael, M. D. Stiles, S. T. B. Goennenwein, and M. Weiler, Spin-torque excitation of perpendicular standing spin waves in coupled YIG/Co heterostructures, *Phys. Rev. Lett.* **120**, 127201 (2018).
- [17] C. D. Stanciu, A. V. Kimel, F. Hansteen, A. Tsukamoto, A. Itoh, A. Kiriljuk, and T. Rasing, Ultrafast spin dynamics across compensation points in ferrimagnetic GdFeCo : The role of angular momentum compensation, *Phys. Rev. B* **73**, 220402(R) (2006).
- [18] Y. Li, Z. Zhang, C. Liu, D. Zheng, B. Fang, C. Zhang, A. Chen, Y. Ma, C. Wang, H. Liu, K. Shen, A. Manchon, J. Q. Xiao, Z. Qiu, C.-M. Hu, and X. Zhang, Reconfigurable spin current transmission and magnon-magnon coupling in hybrid ferrimagnetic insulators, *Nat. Commun.* **15**, 2234 (2024).
- [19] I. Ng, R. Liu, Z. Ren, S. K. Kim, and Q. Shao, Survey of temperature dependence of the damping parameter in the ferrimagnet $\text{Gd}_3\text{Fe}_5\text{O}_{12}$, *IEEE Trans. Magn.* **58**, 1 (2022).
- [20] Y. Li, D. Zheng, B. Fang, C. Liu, C. Zhang, A. Chen, Y. Ma, K. Shen, H. Liu, A. Manchon, and X. Zhang, Unconventional spin pumping and magnetic damping in an insulating compensated ferrimagnet, *Adv. Mater.* **34**, 2200019 (2022).
- [21] C. Kittel, *Introduction to Solid State Physics*, 8th ed. (Wiley, Hoboken, 2005).
- [22] Y. Tserkovnyak, A. Brataas, and G. E. W. Bauer, Enhanced Gilbert damping in thin ferromagnetic films, *Phys. Rev. Lett.* **88**, 117601 (2002).
- [23] J. Sinova, S. O. Valenzuela, J. Wunderlich, C. H. Back, and T. Jungwirth, Spin Hall effects, *Rev. Mod. Phys.* **87**, 1213 (2015).
- [24] S. Geprägs, A. Kehlberger, F. D. Coletta, Z. Qiu, E.-J. Guo, T. Schulz, C. Mix, S. Meyer, A. Kamra, M. Althammer, H. Huebl, G. Jakob, Y. Ohnuma, H. Adachi, J. Barker, S. Maekawa, G. E. W. Bauer, E. Saitoh, R. Gross, S. T. B. Goennenwein, and M. Kläui, Origin of the spin Seebeck effect in compensated ferrimagnets, *Nat. Commun.* **7**, 10452 (2016).
- [25] K.-i. Uchida, H. Adachi, T. Ota, H. Nakayama, S. Maekawa, and E. Saitoh, Observation of longitudinal spin-Seebeck effect in magnetic insulators, *Appl. Phys. Lett.* **97**, 172505 (2010).
- [26] M. Schreier, F. Kramer, H. Huebl, S. Geprägs, R. Gross, S. T. B. Goennenwein, T. Noack, T. Langner, A. A. Serga, B. Hillebrands, and V. I. Vasyuchka, Spin Seebeck effect at microwave frequencies, *Phys. Rev. B* **93**, 224430 (2016).
- [27] See Supplemental Material at <http://link.aps.org/supplemental/10.1103/7d4q-j8cl> for details of the micromagnetic simulation and macrospin model, STEM characterization of the interface quality, extraction of the damping parameter of the single YIG film, and additional resonance spectra of the GdIG layer, which also contains Refs. [34,38].
- [28] M. L. Schneider, J. M. Shaw, A. B. Kos, T. Gerrits, T. J. Silva, and R. D. McMichael, Spin dynamics and damping in nanomagnets measured directly by frequency-resolved magneto-optic Kerr effect, *J. Appl. Phys.* **102**, 103909 (2007).
- [29] I. S. Maksymov and M. Kostylev, Broadband stripline ferromagnetic resonance spectroscopy of ferromagnetic films, multilayers and nanostructures, *Physica E* **69**, 253 (2015).
- [30] H. Maier-Flaig, S. T. B. Goennenwein, R. Ohshima, M. Shiraishi, R. Gross, H. Huebl, and M. Weiler, Note: Derivative divide, a method for the analysis of broadband ferromagnetic

- resonance in the frequency domain, *Rev. Sci. Instrum.* **89**, 076101 (2018).
- [31] S. Funada, D. Kan, K. Kuwano, Y. Shiota, R. Hisatomi, T. Moriyama, Y. Shimakawa, and T. Ono, Low ferrimagnetic damping in $\text{Gd}_3\text{Fe}_5\text{O}_{12}$ epitaxial films grown using pulsed laser deposition, *Appl. Phys. Lett.* **121**, 092402 (2022).
- [32] A. Vansteenkiste, J. Leliaert, M. Dvornik, M. Helsen, F. Garcia-Sanchez, and B. Van Waeyenberge, The design and verification of MuMax3, *AIP Adv.* **4**, 107133 (2014).
- [33] M. Beg, M. Lang, and H. Fangohr, Ubermag: Toward more effective micromagnetic workflows, *IEEE Trans. Magn.* **58**, 1 (2022).
- [34] L. Dreher, M. Weiler, M. Pernpeintner, H. Huebl, R. Gross, M. S. Brandt, and S. T. B. Goennenwein, Surface acoustic wave driven ferromagnetic resonance in nickel thin films: Theory and experiment, *Phys. Rev. B* **86**, 134415 (2012).
- [35] A. Prabhakar and D. D. Stancil, *Spin Waves: Theory and Applications* (Springer US, Boston, MA, 2010).
- [36] Y. S. Chun and K. M. Krishnan, Interlayer perpendicular domain coupling between thin Fe films and garnet single-crystal underlayers, *J. Appl. Phys.* **95**, 6858 (2004).
- [37] G. Venkat, H. Fangohr, and A. Prabhakar, Absorbing boundary layers for spin wave micromagnetics, *J. Magn. Magn. Mater.* **450**, 34 (2018).
- [38] T. D. Rossing, Resonance linewidth and anisotropy variation in thin films, *J. Appl. Phys.* **34**, 995 (1963).
- [39] R. Kumar, B. Samantaray, S. Das, K. Lal, D. Samal, and Z. Hossain, Damping in yttrium iron garnet films with interface, *Phys. Rev. B* **106**, 054405 (2022).
- [40] G. F. Dionne, *Magnetic Oxides* (Springer, New York, 2009).
- [41] M. Belmeguenai, T. Martin, G. Woltersdorf, M. Maier, and G. Bayreuther, Frequency- and time-domain investigation of the dynamic properties of interlayer-exchange-coupled $\text{Ni}_{81}\text{Fe}_{19}/\text{Ru}/\text{Ni}_{81}\text{Fe}_{19}$ thin films, *Phys. Rev. B* **76**, 104414 (2007).
- [42] A. B. Drovoskov, D. I. Kholin, and N. M. Kreinies, Magnetic properties of layered ferrimagnetic structures based on Gd and transition 3d metals, *J. Expt. Theor. Phys.* **131**, 149 (2020).
- [43] J. Cramer, E.-J. Guo, S. Geprägs, A. Kehlberger, Y. P. Ivanov, K. Ganzhorn, F. Della Coletta, M. Althammer, H. Huebl, R. Gross, J. Kosel, M. Kläui, and S. T. B. Goennenwein, Magnon mode selective spin transport in compensated ferrimagnets, *Nano Lett.* **17**, 3334 (2017).
- [44] Y. Ohnuma, H. Adachi, E. Saitoh, and S. Maekawa, Spin Seebeck effect in antiferromagnets and compensated ferrimagnets, *Phys. Rev. B* **87**, 014423 (2013).
- [45] T. An, V. I. Vasyuchka, K. Uchida, A. V. Chumak, K. Yamaguchi, K. Harii, J. Ohe, M. B. Jungfleisch, Y. Kajiwara, H. Adachi, B. Hillebrands, S. Maekawa, and E. Saitoh, Unidirectional spin-wave heat conveyer, *Nat. Mater.* **12**, 549 (2013).
- [46] J. Cheng, K. He, M. Yang, Q. Liu, R. Yu, L. Sun, J. Ding, B. Miao, M. Wu, and H. F. Ding, Quantitative estimation of thermoelectric contributions in spin pumping signals through microwave photoresistance measurements, *Phys. Rev. B* **103**, 014415 (2021).
- [47] Y. Fan, P. Quarterman, J. Finley, J. Han, P. Zhang, J. T. Hou, M. D. Stiles, A. J. Grutter, and L. Liu, Manipulation of coupling and magnon transport in magnetic metal-insulator hybrid structures, *Phys. Rev. Appl.* **13**, 061002(R) (2020).
- [48] A. Kamra, R. E. Troncoso, W. Belzig, and A. Brataas, Gilbert damping phenomenology for two-sublattice magnets, *Phys. Rev. B* **98**, 184402 (2018).
- [49] F. Fuhrmann, S. Becker, A. Akashdeep, Q. Lan, N. Wang, R. E. Dunin-Borkowski, R. Lebrun, M. Weiler, G. Jakob, and M. Kläui, Data set for the article “Temperature-dependent study of the spin dynamics of coupled $\text{Y}_3\text{Fe}_5\text{O}_{12}/\text{Gd}_3\text{Fe}_5\text{O}_{12}/\text{Pt}$ trilayers,” Zenodo (2025), doi: [10.5281/zenodo.16037744](https://doi.org/10.5281/zenodo.16037744).